



Islamic Azad University



Research Paper

Designing an electro-optical 8-to-3 encoder based on resonant cavity and graphene- Al_2O_3 stack in the photonic crystal platform

Fatemeh Haddadan^{1,2,*}, Mohammad Soroosh², Jaspal Singh³

1. Department of Electrical Engineering, Karoon Institute of Higher Education, Ahvaz, Iran
2. Department of Electrical Engineering, Shahid Chamran University of Ahvaz, Ahvaz, Iran
3. Laboratory of Advanced Materials for Energy and Environment, Department of chemistry, biochemistry, and Physics, University of Quebec at Trois-Rivieres, 3351, boul. des Forges, C.P. 500, Trois-Rivières (Québec), Canada, G9A 5H7

Received: 12 Sep. 2024

Revised: 21 Oct. 2024

Accepted: 30 Oct. 2024

Published: 15 Nov. 2024

Abstract

Here, a new optical 8-to-3 encoder based on the photonic crystal resonant cavity and graphene- Al_2O_3 stack is proposed. To control the light transmission, a resonant cavity parallel to the waveguide in a one-dimensional platform is utilized. Some air holes are assumed near the cavity for achieving an interference, and generating a notch filter at a resonance wavelength of $1.49 \mu\text{m}$. To control the filter's quality factor, a graphene- Al_2O_3 stack is used at the cavity center. Dependency of the dielectric constant and the refractive index of the stack to the graphene chemical potential makes a possibility to modulate the light transmission through the waveguide. The pair of the waveguide and the photonic crystal cavity acts as an electro-optical switch, where its operation depends on the applied voltage to the stack. Five electro-optical switches are employed to control the light passing from input ports toward three output ports. The area and the contrast ratio are $150 \mu\text{m}^2$ and 11.62 dB, respectively. The modulation depth of 97.6% and the crosstalk of -14.63 dB are additional advantages of the designed encoder. The tuneability of the transmission efficiency for the designed switches as the basis block is an interesting feature of the designed encoder. Also, the proposed structure can be easily extended to higher orders which is highly needed for optical circuits and optical networks.

Keywords:

Contrast ratio,
Electro-optical encoder,
Graphene,
Photonic crystal,
Resonant cavity

Citation: Fatemeh Haddadan, Mohammad Soroosh, Jaspal Singh. Designing an electro-optical 8-to-3 encoder based on resonant cavity and graphene- Al_2O_3 stack in the photonic crystal platform. **Journal of Optoelectrical Nanostructures**. 2024; 9 (4): 21-38. DOI: [10.30495/JOPN.2024.33689.1328](https://doi.org/10.30495/JOPN.2024.33689.1328)

Corresponding author: Fatemeh Haddadan

Address: Department of Electrical Engineering, Karoon Institute of Higher Education, Ahvaz, Iran. **Tell:** +989363318386 **Email:** f.haddadan@scu.ac.ir

1. INTRODUCTION

Photonic crystal cavities (PCCs) possess high quality factors due to effective interaction between light and matter, covering various modes. These elements find applications in quantum information processing, nonlinear optics, optical telecommunication, and photonic fluids [1-3]. The diameter of the holes and the periodic length of the photonic crystal can be adjusted to achieve high quality factors [4-5].

Graphene exhibits attractive optical and electrical properties such as very high mobility and tunable absorption of light over a wide bandwidth [6-7]. Experimental results have shown that the surface conductivity of graphene can be effectively tuned via electrical biasing, magnetic fields, or chemical doping. This capability enables solving the non-tunability issue of hardware and achieving dynamic control of wavelength across the mid-infrared and far-infrared regions [4,8].

Waveguides are used in photonic circuits for transmitting and sharing optical signals. This function can also be performed for encoders, which include logical gates [9]. Various structures based on photonic crystals have been proposed for encoding purposes [4,10-24]. Lee et al. proposed a 4-to-2 encoder based on silicon rods arranged in a triangular lattice in an air background [12]. This structure utilized Y-shaped waveguides and point defects. Although normalized output power levels for logic 0 and 1 were 5% and 98%, respectively, the large size of the structure did not seem suitable for integration.

Moniem proposed an encoder based on photonic crystals using square-lattice silicon rods. The encoder's operation was based on NOR logic gates and four ring resonators [18]. Unlike previous research, the time response of the structure was analyzed. Rise and fall times were approximately 2 ps and 1.3 ps, respectively. Hassangholizadeh-Kashtiban et al. presented an encoder using elliptical ring resonators and nonlinear rods with rod diameters and minimum spacing of 106 nm and 100 nm, respectively [16]. Another 4-to-2 encoder was proposed by Ouahab et al. which included cavities and L-shaped waveguides [14]. A similar structure was proposed by Mehdizadeh et al. reducing the rise time to less than 1 ps but with a structure size of 880 μm^2 [13]. Gholamnejad et al. proposed a different structure using GaAs rods in a square lattice with two ring resonators and biasing ports [19]. Naghizade et al. proposed an encoder using OR logic gates and ring resonators claiming correct encoder operation but one inactive output port for the state 11 [15]. Seif-Dargahi proposed a 4-to-2 encoder with four ring resonators and an area of 722 μm^2 [17]. Parandin

proposed a 4-to-2 encoder using a square arrangement of two-dimensional photonic crystals and some defects [21].

These structures utilized various materials such as silicon [25], GaAs [26-27], chalcogenide [28], and polystyrene [29], each with specific properties that cannot be altered after fabrication [30, 31]. In this research, graphene is used in the photonic crystal for designing a 4-to-2 encoder. By altering the applied voltage to this material, its chemical potential, dielectric constant, absorption coefficient, and refractive index change. A multilayer graphene- Al_2O_3 is used as the rod stack. To control light transmission from a silicon waveguide, a waveguide 70 nm away from it with 20 air holes is designed as a cavity resonator for the input light wavelength. Placing a multilayer graphene- Al_2O_3 at the center of the cavity enables control of optical signal transmission by adjusting the graphene chemical potential. The ability to adjust the chemical potential of graphene is the most significant advantage of the proposed structure compared to the mentioned structures. The footprint of the device is equal to $150 \mu\text{m}^2$. For an input light wavelength of $1.49 \mu\text{m}$, the normalized output powers for logic 0 and 1 are 3.1% and 45%, respectively. The modulation depth of 97.6% and the crosstalk of -14.63 dB are additional advantages of the designed encoder.

Section 2 introduces the designed 8-to-3 encoder based on a fundamental electro-optical switch. In this section, the structure is simulated and the components of electric and magnetic fields are calculated throughout the device for 8 working states. Finally, the conclusion of this study is summarized.

2. THE PROPOSED 8-TO-3 ENCODER

To design the proposed 8-to-3 encoder, it needs to create a structure with five optical bias ports, two dividers, three combiners and three output ports. The connection of waveguides links the optical bias waveguides to the output ports by the help of the combiners in a manner that allows the overall structure to function as an 8-to-3 encoder. The proposed structure is illustrated in Figure 1. As depicted, the waveguides W_1 and W_6 connect the optical bias to output port O_0 . Waveguides W_6 and W_7 , through the divider, connects waveguide W_2 to output ports O_0 and O_1 , respectively. Waveguides W_3 and W_7 guide the incoming waves toward the port O_1 . The divider links waveguide W_4 through W_7 and W_8 to output port O_1 and O_2 , respectively. The waveguides W_5 and W_8 connect directly the optical signal to the port O_2 . It is noteworthy five optical waveguides W_1 to W_5 are situated near five cavities with the chemical potentials μ_1 to μ_5 , respectively. A set of a waveguide and its near cavity functions as an

electro-optical switch described as follow.

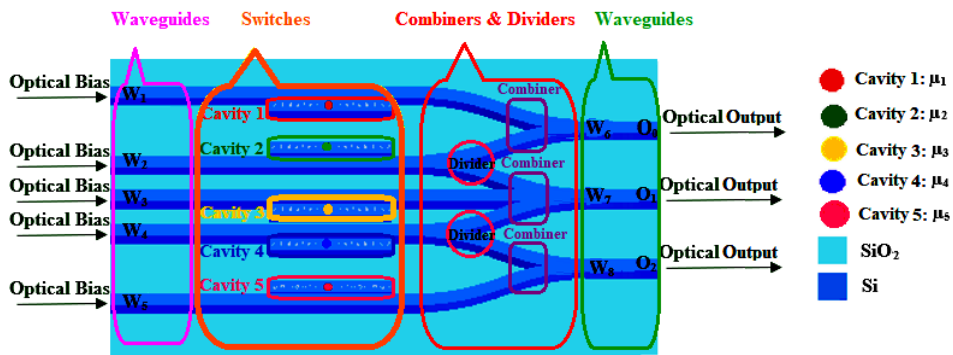


Fig. 1. A view of the proposed 8-to-3 electro-optical encoder including 8 waveguides, 2 dividers, 3 combiners and 5 resonant cavities as electro-optical switches for directing optical biases toward ports O_0 , O_1 , and O_2 .

Figure 2 depicts the structure of an electro-optical switch where the passage of light through a waveguide is controlled by altering the chemical potential of graphene layers. The structural parameters are provided in Figure 2. The switch consists of a silicon waveguide located 70 nm away from a resonant cavity photonic crystal. The waveguide and cavity have widths and heights of 500 nm and 260 nm, respectively, and are considered on an SiO_2 substrate. At the center of the photonic crystal cavity, there is a graphene- Al_2O_3 stack composed of 8 graphene monolayers, each 1 nm thick, sandwiched between Al_2O_3 layers. The radius of these layers is 100 nm. The proposed structure features air holes in sections A, B, and C on both sides of the graphene stack, symmetrically arranged around the cavity center (see Figure 2).

The close proximity of the cavity to the waveguide enables efficient optical coupling, while the reflections from the air holes create a resonant cavity that controls the amount of light transmitted through the waveguide. By adjusting the chemical potential of graphene, we can change its dielectric constant and refractive index, thereby influencing the properties of the entire stack. Consequently, the interference of forward and backward waves in the cavity also changes, affecting the amount of light transmitted through the waveguide.

The finite-difference time-domain (FDTD) method is a numerical simulation tool that solves Maxwell's equations to model electromagnetic wave propagation. It's widely used in engineering and physics to simulate how electromagnetic fields interact with materials and structures. In this case, the FDTD method was used to simulate the propagation of optical waves within the proposed structure. The method calculates the electric and magnetic field

components in both space and time. The cell dimensions in three dimensions (Δx , Δy , and Δz) are set to 0.25 nm smaller than the wavelength [32].

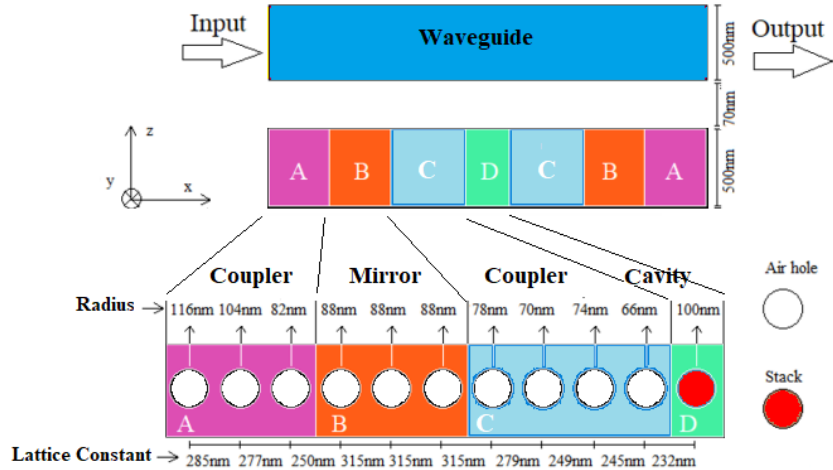


Fig. 2. The fundamental electro-optical switch for light transmission through the waveguide. The resonant cavity includes a graphene-Al₂O₃ stack at the center along with air holes positioned at two sides symmetrically.

The Courant condition which is a critical parameter in numerical simulations, particularly those involving partial differential equations such as the FDTD method, the time step (Δt) should satisfy the following equation [32]:

$$1 \leq \sqrt{\frac{\Delta x^2 + \Delta y^2 + \Delta z^2}{3c^2\Delta t^2}} \tag{1}$$

where the light velocity in vacuum is denoted by c . Therefore, a time step of 29.2 as is assumed to the simulation. The perfectly matched layer (PML) is applied as the crucial condition due to the proximity of the resonant cavity and the optical waveguide. The layer is designed to absorb electromagnetic waves efficiently across a wide range of frequencies. This prevents unwanted reflections that can interfere with the simulated results. A layer of material with gradually increasing conductivity is placed around the simulation domain. As electromagnetic waves propagate towards the PML, they are absorbed by the conductive material, minimizing reflections. The PML is designed to have an impedance that matches the impedance of the surrounding medium, ensuring minimal reflections. The transfer matrix model is used in many engineering and scientific applications, particularly in optics and electronics, for its ability to describe the transmission and reflection properties of complex systems. The transfer matrix model described in [33] can be utilized for analysis.

Additionally, a theory of coupling is employed to determine the transmission efficiency (T) for resonance frequency (ω_0) [33].

$$T(\omega_0) = \frac{4\tau_1\tau_2}{(\tau_1 + \tau_2 + \tau_a + \tau_r)^2} \quad (2)$$

where τ_1 , τ_2 , τ_r and τ_a are the coupling rate to the input port, output port, the radiation loss rate and absorption rate of the PC-based cavity, respectively. The absorption coefficient (A) for resonance state can be calculated as follows [33]:

$$A(\omega_0) = \frac{4\tau_1\tau_a}{(\tau_1 + \tau_2 + \tau_a + \tau_r)^2} \quad (3)$$

In an ideal scenario, radiation loss would be minimal and negligible. Therefore, assuming the operating frequency (ω) remains constant ($\omega=\omega_0$), it can analyze the transmission and absorption properties for different values of τ_1/τ_a and τ_2/τ_a (relaxation times). Figure 3 illustrates that both transmission and absorption increase as τ_1/τ_a and τ_2/τ_a rise. However, there's a limit to this effect. At the resonance frequency of the incoming light wave, τ_1 and τ_2 become relatively small. In simpler terms, if τ_1 is equal to τ_a and τ_a is much larger than τ_2 (as shown in Figure 3), absorption surpasses 25%. This condition is known as critical coupling [34]. The key takeaway is that this structure offers electrical tuning by manipulating the absorption within the photonic crystal section. For efficient tunability, prior research suggests using a graphene- Al_2O_3 stack with more than three graphene layers [33]. Therefore, this paper assumes that the stack has eight graphene layers.

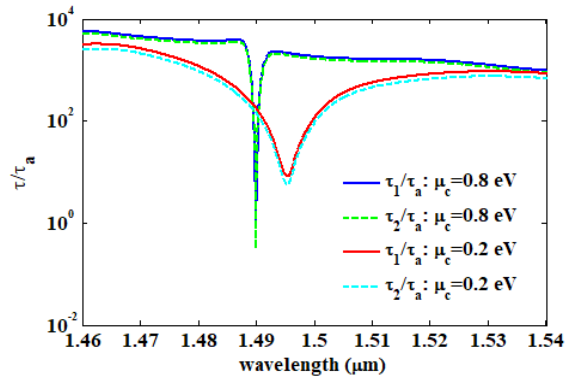


Fig. 3. Rate ratio τ_1/τ_a and τ_2/τ_a for two states; $\mu_c=0.8$ eV and $\mu_c=0.2$ eV versus wavelength.

When an electric field is applied to the graphene- Al_2O_3 stack, it changes the chemical potential of the graphene layer. Additionally, the number of graphene layers in the stack affects how light waves interact within the structure. This

effect is due to the variations in the overall permittivity of the stack, which can be calculated using effective medium theory, as described in reference [35]:

$$\varepsilon_{\parallel} = \varepsilon_d + \frac{j\sigma}{\omega\varepsilon_0 h_d} \quad (4a)$$

$$\varepsilon_{\perp} = \varepsilon_d \quad (4b)$$

where ε_0 , ε_{\parallel} , and ε_{\perp} denote the free space permittivity, the parallel and normal parts of permittivity in the xz -plane, respectively. In this design, the graphene monolayers are separated by thin insulating spacer layers made of Al_2O_3 with a thickness of 28 nm ($h_d=28$ nm) and a relative permittivity of 3.05 ($\varepsilon_d = 3.05$). From an electrical standpoint, a single layer of graphene behaves like a 2d material with a characteristic surface conductivity denoted by σ [36]. This surface conductivity can be calculated using Kubo's formula and comprises two main parts: σ_{inter} , which arises from transitions between different electron energy bands, and σ_{intra} , which originates from transitions within the same band [37].

$$\sigma_{\text{inter}} = \frac{-jq^2(\omega + j2\tau^{-1})}{\pi\hbar^2} \int_0^{\infty} \xi \left(\frac{f_d(-\xi) - f_d(\xi)}{(\omega + j2\tau^{-1})^2 - (2\xi/\hbar)^2} \right) d\xi \quad (5a)$$

$$\sigma_{\text{intra}} = \frac{-jq^2}{\pi\hbar^2(\omega + j2\tau^{-1})} \int_0^{\infty} \xi \left(\frac{\partial f_d(\xi)}{\partial \xi} - \frac{\partial f_d(-\xi)}{\partial \xi} \right) d\xi \quad (5b)$$

$$f_d(\xi) = \frac{1}{\exp((\xi - \mu_c)/(k_B T)) + 1} \quad (5c)$$

where τ , μ_c , q , \hbar , T , and k_B denote the relaxation time, the graphene chemical potential, the electron charge, the reduced plank constant, the temperature in Kelvin, and Boltzmann constant. The thickness of graphene is assumed to be 0.35 nm in this study.

Figure 4a shows the real and imaginary parts of the permittivity for various graphene chemical potential values. As observed, the real part of ε_{\parallel} (permittivity parallel to the layers) initially rises with increasing chemical potential, followed by a decrease. This behavior aligns with the typical characteristics of graphene, as detailed in reference [38]. The imaginary component of ε_{\parallel} exhibits a significant decrease within the narrow range of chemical potential between 0.4 eV and 0.6 eV. In contrast, for other chemical potential values, this change is more gradual. This behavior is linked to the Pauli exclusion principle, which comes into play for μ_c exceeding 0.4 eV (chemical potential greater than 0.4 eV). Electrons in graphene transition from the valence band to the conduction band as the chemical potential rises. However, due to the Pauli exclusion principle, this transition is limited, causing the absorption coefficient to decrease. This reduction in absorption leads to graphene becoming more transparent to incoming light, as observed in [38].

With the variation of the chemical potential of graphene, the wave transmission efficiency changes, as depicted in Figure 4b. For $\mu_c > 0.4$ eV, amplification in the photonic crystal cavity leads to severe destruction of the transmitted light through the waveguide, creating a stop band. Conversely, for chemical potentials less than 0.4 eV, the imaginary part of the refractive index in the graphene- Al_2O_3 stack increases exponentially, enhancing the absorption coefficient and reducing its destructive effect. Therefore, the output light range from the waveguide increases along the resonant wavelength. This concept is utilized as an idea to achieve switching functionality. In addition to changes in light transmission due to refractive index variations, changes in the resonance wavelength are observed.

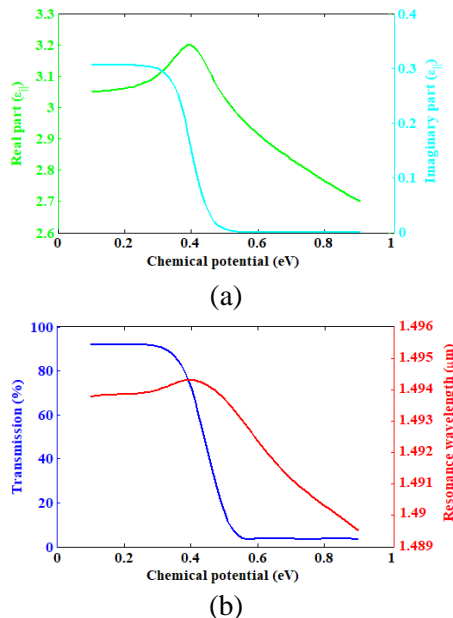


Fig. 4. (a) The real and imaginary parts of the stack permittivity for the chemical potential (b) The resonance wavelength along with transmission in terms of the graphene chemical potential ranges from 0.1 eV to 0.9 eV.

Figure 5 shows the electric field distribution of the optical waves in the xz -plane at a wavelength of 1.49 μm . It can be observed that for a chemical potential of 0.2 eV, the majority of the input signals are transmitted through the waveguide. However, at a chemical potential of 0.8 eV, a significant portion of the light is concentrated in the center of the photonic crystal. The graphene- Al_2O_3 stack along with the air holes create a stop band due to destructive interference in the resonance wavelength. As a result, the incoming bias does

not reach the end of the waveguide.

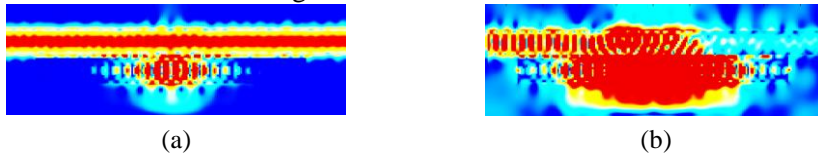


Fig. 5. The electric field components of the optical bias in the x and the z directions at a wavelength of 1.49 μm for (a) $\mu_c=0.2$ eV and (a) $\mu_c=0.8$ eV.

Based on the findings for the designed electro-optical switch, it seems feasible to design an 8-to-3 encoder using the resonance phenomenon in PCC. Therefore, by adjusting μ_c , the transmission of light through the waveguide can be significantly controlled. This concept shows a new way for achieving encoding functionality. Figure 6 illustrates how the propagation of optical waves varies with different chemical potential states for an encoder. The operation of an encoder works such that at any given moment, only one of its inputs can be logical, and correspondingly, its binary code is generated at the output ports. For this reason, eight operational states have been simulated for the given structure in Figure 1 as described below.

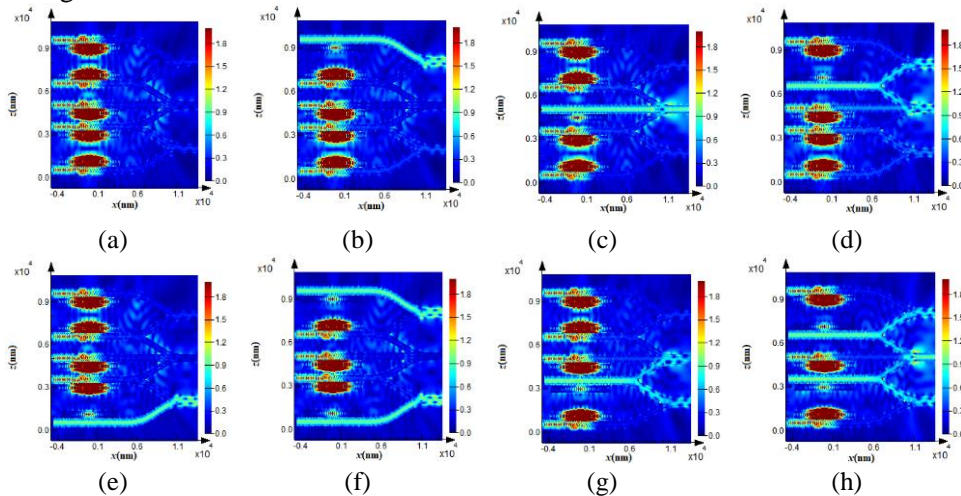


Fig. 6. A presentation of the electric field distribution for achieving the encoding operation for 8 states (a) 1, (b) 2, (c) 3, (d) 4, (e) 5, (f) 6, (g) 7, and (h) 8.

State 1: in this state, all stacks have a chemical potential of 0.8 eV. All optical waves experience a destructive interference. So, all waveguides do not transmit waves (as shown in Figure 6a). All output ports O_0 , O_1 , and O_2 remain at logic 0 with $O_2O_1O_0=000$ representing the working state.

State 2: Assuming $\mu_1=0.2$ eV for the stack near W_1 and 0.8 eV for other

stacks, optical waves pass through W_1 and W_6 towards port O_0 (see Figure 6b). Here, port O_0 is activated while others remain inactive, generating code 001 at ports O_2 , O_1 , and O_0 , respectively.

State 3: As illustrated in Figure 6c, with $\mu_3=0.2$ eV and $\mu_1=\mu_2=\mu_4=\mu_5=0.8$ eV, SPPs through W_3 , W_7 are transmitted toward O_1 , generating code 010 at ports O_2 , O_1 , and O_0 , respectively.

State 4: If only μ_2 equals 0.2 eV, both ports O_1 and O_0 are activated. In this circumstance, W_2 transmits optical waves toward O_0 and O_1 through W_6 and W_7 , respectively, resulting in $O_2O_1O_0=011$ (as depicted in Figure 6d)

State 5: With $\mu_5=0.2$ eV and $\mu_1=\mu_2=\mu_3=\mu_4=0.8$ eV, bias signals through W_5 and W_8 are guided toward O_2 , and generate code 100 at a form of $O_2O_1O_0$ (see Figure 6e).

State 6: For $\mu_1=\mu_5=0.2$ eV and $\mu_2=\mu_3=\mu_4=0.8$ eV, optical waves transmit through W_1 and W_5 , and reach port O_0 and O_2 through W_6 and W_8 , generating code 101 for $O_2O_1O_0$ (as shown in Figure 6f).

State 7: If only μ_4 equals 0.2 eV, both ports O_2 and O_1 are activated. In this state, W_4 transmits incoming waves toward O_1 and O_2 through W_7 and W_8 , respectively, resulting in code 110 (as illustrated in Figure 6g).

State 8: With $\mu_2=\mu_4=0.2$ eV and $\mu_1=\mu_3=\mu_5=0.8$ eV, waves transfer through W_2 and W_4 and are guided toward O_0 , O_1 , and O_2 through W_6 , W_7 , and W_8 , generating a binary code of $O_2O_1O_0=111$ as shown in Figure 6h.

Table I provides further details on states 1 to 8 as mentioned, including normalized power details at the output ports. In each state, based on the graphene's chemical potential, some waveguides transfer the optical signals to the outputs. As illustrated in Figure 5, selecting a graphene chemical potential of 0.2 eV enables input light to propagate through the waveguide, whereas a chemical potential of 0.8 eV blocks input waves with a wavelength of 1.49 μm . As shown in Figures 3 and 6, controlling the graphene's chemical potential within the stack allows us to regulate light transmission through the waveguide. Our findings demonstrate that a maximum of 3.1% of the normalized power reaches one output port, establishing a threshold for logic 0 ($M_0 = 3.1\%$). Conversely, the minimum normalized transmission value is 45%, which sets the threshold for logic 1 ($M_1 = 45\%$). Based on this on/off ratio, the structure achieves a contrast ratio (CR) of 11.62 dB, calculated using the formula $10 \times \log(M_1/M_0)$.

TABLE I
The obtained results of the designed 8-to-3 electro-optical encoder.

State	Chemical potential (eV)					Guiding through waveguides	Output port					
	μ_1	μ_2	μ_3	μ_4	μ_5		Logic			Normalized transmission (%)		
							O_2	O_1	O_0	O_2	O_1	O_0
1	0.8	0.8	0.8	0.8	0.8	-	0	0	0	2.2	3.1	2.2
2	0.2	0.8	0.8	0.8	0.8	W_1, W_6	0	0	1	2.2	3.1	90
3	0.8	0.8	0.2	0.8	0.8	W_3, W_7	0	1	0	2.2	90	2.2
4	0.8	0.2	0.8	0.8	0.8	W_2, W_6, W_7	0	1	1	2.3	45.8	45
5	0.8	0.8	0.8	0.8	0.2	W_5, W_8	1	0	0	90	3.1	2.2
6	0.2	0.8	0.8	0.8	0.2	W_1, W_5	1	0	1	90	3.1	90
7	0.8	0.8	0.8	0.2	0.8	W_4, W_7, W_8	1	1	0	45	45.8	2.2
8	0.8	0.2	0.8	0.2	0.8	W_2, W_4, W_6, W_7, W_8	1	1	1	45	91.6	45

Modulation depth is a critical parameter in graphene-based waveguides used for binary recognition in encoders. It directly influences the accuracy and reliability of the encoding process. A higher modulation depth results in a more pronounced difference between the "on" and "off" states of the optical signal. This clarity is essential for accurate binary recognition. A well-modulated signal is easier to decode correctly by the encoder's receiver, reducing the likelihood of errors in the binary data.

The performance of the encoder was assessed by comparing its area, contrast ratio, modulation depth (MD), and crosstalk (CT) to those reported in other studies [4,10-21]. The results are summarized in table II. Previous studies [10-19] on two-dimensional photonic crystals utilized all-optical (AO) mechanisms, requiring additional optical ports to enhance the contrast ratio. These structures operated in nonlinear regimes, exhibiting the optical Kerr effect. In contrast, the proposed electro-optical (EO) device does not involve nonlinear effects and achieves a smaller area compared to the prior works. References [10,12-21] are related to 4-to-2 encoders while the introduced device is 8-to-3. As far as we know, the presented structure is the first optical PC-based encoder that show a way to researchers to extend their structures. Really, the designed structure can be also extended while some above-mentioned references have not this feature because of the limitation in cross-connections for two-dimensional PC structures. The excellent feature of the introduced structure for encoding operation is the tunability of graphene. Controlling the passing of the optical bias by changing the graphene chemical potential may help to compensate a part

of errors in fabrication of the device. It is noteworthy that the modulation depth in the designed encoder is larger than that of references [4,15,17].

The comparison of the obtained crosstalk with that of references [4,11,13,16-17] reveals that lower crosstalk has been achieved in a smaller area. This is a significant advantage of the proposed encoder. Regarding device integration, the crosstalk challenge is a major issue in design, so the presented idea offers a promising solution to reduce the crosstalk problem.

TABLE II
Comparison of the proposed structure with other structures.

Work	Encoding form	Area (μm^2)	CR (dB)	MD (%)	CT (dB)
[4]		127	7.6	91	-10.36
[10]		612	16.33	98.04	-17.08
[12]		880	7.32	-	-
[13]		880	12.92	99.9	-10.41
[14]		757	9.54	-	-
[15]	4-to-2	723	11.76	96.84	-15.01
[16]		200	9.03	-	-9.91
[17]		792	9.2	93.33	-11.76
[18]		1225	-	-	-
[19]		744	17.78	-	-
[20]		150	13.76	97.78	-16.53
[21]		132.7	16.53	97.8	-16.53
[11]	8-to-3	510	5.74	98	-11.76
This work		150	11.62	97.6	-14.63

The structure controls light transmission through the designed waveguides by adjusting μ_c . The feasibility of building such a structure is supported by previous research. Zain et al., for example, successfully created one-dimensional photonic crystal cavities in silicon-on-insulator using a single-step electron-beam lithography (EBL) process [39]. Their technique involved defining the waveguide pattern with a negative resist layer and etching cavities with varying air hole sizes. Yan et al. analyzed insulator-graphene layers for use as notch filters, demonstrating an extinction of 9.5 dB [40]. Their process involved depositing graphene, doping it, and patterning the multilayer structure. For fabricating a graphene- Al_2O_3 stack, alternating layers can be deposited sequentially, followed by patterning using EBL and inductive coupling plasma as described in [40-41]. These successful demonstrations provide strong optimism for the feasibility of creating the proposed modulator.

3. CONCLUSION

In this study, a photonic crystal-based 8-to-3 encoder comprising 5 electro-optical switches has been designed. Each switch consists of a photonic crystal resonant cavity placed near the waveguide. The resonant cavity includes one graphene- Al_2O_3 stack at the center of the cavity and 20 air holes. The height of the graphene layers is equal to 1 nm and their radii equals 0.1 μm . Bragg reflections from holes and stack make an interference pattern in the cavity. The findings demonstrate a graphene chemical potential 0.2 eV allows 90% of the incoming power to be traveled toward the output at the resonance wavelength. Moreover, the structure results in a contrast ratio of 11.62 dB in a small area of 150 μm^2 . The modulation depth of 97.6% and the crosstalk of -14.63 dB are the other advantages of the designed encoder. The presented device is more compact than the previous structures, and supports 8 working states in a form of 8-to-3 encoder while other works support just 4 states in a larger area. The proposed design demonstrates promising performance as an 8-to-3 electro-optical encoder.

ACKNOWLEDGMENT

This work was supported by Shahid Chamran University of Ahvaz, grant number SCU.EE1402.672.

REFERENCES

- [1] M.J. Maleki, M. Soroosh, F. Parandin, and F. Haddadan, Photonic crystal-based decoders: ideas and structures. *Recent Advances and Trends in Photonic Crystal Technology*. Intech Open. (2023). Available: <https://doi.org/10.5772/intechopen.1002401>
- [2] M.J. Maleki, M. Soroosh, G. Akbarizadeh, F. Parandin, and F. Haddadan. *Photonic crystal resonators in designing optical decoders*. *Journal of Optoelectrical Nanostructures (JOPN)*. 1(57) (2021) 48-57. Available: <https://doi.org/10.30495/JOPN.2023.32220.1296>
- [3] T. Daghooghi, M. Soroosh, and K. Ansari-Asl. *Slow light in ultra-compact photonic crystal decoder*. *Appl. Opt.* 58(8) (2019) 2050–2057. Available: <https://doi.org/10.1364/AO.58.002050>
- [4] F. Haddadan, M. Soroosh, and N. Alaei-Sheini. *Designing an electro-optical encoder based on photonic crystals using the graphene- Al_2O_3 stacks*. *Appl. Opt.* 59(7) (2020) 2179-2185. Available: <https://doi.org/10.1364/AO.386248>

- [5] J. Hendrickson, R. Soref, J. Sweet, and W. Buchwald. *Ultrasensitive silicon photonic-crystal nanobeam electro-optical modulator: Design and simulation*. Opt. Express 22(3) (2014) 3271–3283. Available: <https://doi.org/10.1364/OE.22.003271>
- [6] M. Soroosh, A. Farmani, M.J. Maleki, F. Haddadan, M. Mansouri. Highly efficient graphene-based optical components for networking applications. In *Photonic Crystal and Its Applications for Next Generation Systems*. Singapore: Springer Nature Singapore. (2023) 15-35. Available: https://doi.org/10.1007/978-981-99-2548-3_2
- [7] F. Haddadan, M. Soroosh, and N. Alaei-Sheini. *Cross-talk reduction in a graphene-based ultra-compact plasmonic encoder using an Au nano-ridge on a silicon substrate*. Appl. Opt. 61(11) (2022) 3209-3217. Available: <https://doi.org/10.1364/AO.449123>
- [8] M.H. Liu, C. Gorini, and K. Richter. *Creating and steering highly directional and electron beams in graphene*. Phys. Rev. Lett. 118(6) (2017) 066801. Available: <https://doi.org/10.1103/PhysRevLett.118.066801>
- [9] H.M. Hussein, T.A. Ali, and N.H. Rafat. *A review on the techniques for building all-optical photonic crystal logic gates*. Opt. Laser Technol. 106(1) (2018) 385–397. Available: <https://doi.org/10.1016/j.optlastec.2018.04.018>
- [10] F. Hadadan, and M. Soroosh. *A new proposal for 4-to-2 optical encoder using nonlinear photonic crystal ring resonators*. Int. J. Opt. Photonics 13(2) (2019) 119–126. Available: <https://ijop.ir/article-1-333-en.html>
- [11] F. Haddadan, and M. Soroosh. *Low-power all-optical 8-to-3 encoder using photonic crystal-based waveguides*. Photon. Netw. Commun. 37 (2019) 83–89. Available: <https://doi.org/10.1007/s11107-018-0795-3>
- [12] K.Y. Lee, Y.C. Yang, Y.J. Lin, W.Y. Lee, C.C. Lee, and S.H. Wong. *The designs of 4-2 encoder based on photonic crystals*. Asia Commun. Photonics Conf. Exhib. 2009 (2009) 1–7. Available: <https://ieeexplore.ieee.org/abstract/document/5405478>
- [13] F. Mehdizadeh, M. Soroosh, and H. Alipour-Banaei. *Proposal for 4-to-2 optical encoder based on photonic crystal structure*. IET Optoelectron. 11(1) (2017) 29–35. Available: <https://doi.org/10.1049/iet-opt.2016.0022>
- [14] I. Ouahab, and R. Naoum. *A novel all optical 4-2 encoder switch based on photonic crystal ring resonators*. Optik 127(19) (2016) 7835–7841.

Available: <https://doi.org/10.1016/j.ijleo.2016.05.080>

- [15] S. Naghizade, and H. Khoshshima. *Low input power an all optical 4-2 encoder based on triangular lattice shape photonic crystal*. J. Opt. Commun. 42(1) (2018)17–24. Available: <https://doi.org/10.1515/joc-2018-0019>
- [16] M. Hassangholizadeh-Kashtiban, R. Sabbaghi-Nadooshan, and H. Alipour-Banaei. *A novel all optical reversible 4-2 encoder based on photonic crystals*. Optik 126(20) (2015) 2368–2372. Available: <https://doi.org/10.1016/j.ijleo.2015.05.140>
- [17] H. Seif-Dargahi. *Ultra-fast all-optical encoder using photonic crystal-based ring resonators*. Photon. Netw. Commun. 36(2) (2018) 272–277. Available: <https://doi.org/10.1007/s11107-018-0779-3>
- [18] T.A. Moniem. *All-optical digital 4-2 encoder based on 2D photonic crystal ring resonators*. J. Mod. Opt. 63(8) (2016) 735–741. Available: <https://doi.org/10.1080/09500340.2015.1094580>
- [19] S. Gholamnejad, and M. Zavvari. *Design and analysis of all-optical 4–2 binary encoder based on photonic crystal*. Opt. Quantum Electron. 49(302) (2017) 302–313. Available: <https://doi.org/10.1007/s11082-017-1144-y>
- [20] S. Naghizade and H. Saghaei. *A novel design of all-optical 4 to 2 encoder with multiple defects in silica-based photonic crystal fiber*. Optik 222 (2020) 165419. Available: <https://doi.org/10.1016/j.ijleo.2020.165419>
- [21] F. Parandin. *High contrast ratio all-optical 4×2 encoder based on two dimensional photonic crystals*. Opt. Laser Technol. 113 (2019) 447–452. Available: <https://doi.org/10.1016/j.optlastec.2019.01.003>
- [22] H. Alipour-Banaei, M.G. Rabati, P. Abdollahzadeh-Badelbou, and F. Mehdizadeh. *Application of self-collimated beams to realization of all optical photonic crystal encoder*. E Low-Dimens. Syst. Nanostruct. 75 (2016) 77–85. Available: <https://doi.org/10.1016/j.physe.2015.08.011>
- [23] D. Zhang, and G. You. *Miniaturization design of all-optical encoder based on surface design and radiation source control*. Phys. E Low-Dimens. Syst. Nanostruct. 127 (2021) 114469. Available: <https://doi.org/10.1016/j.physe.2020.114469>

- [24] K. Latha, R. Arunkumar, K. Rama Prabha, and S. Robinson. *Performance analysis of all optical 4*2 and 8*3 encoder using two dimensional photonic crystals waveguides*. Silicon 14 (2022) 3245–3258. Available: <https://doi.org/10.1007/s12633-021-01107-2>
- [25] F. Pakrai, M. Soroosh, and J. Ganji. *Designing of all-optical subtractor via PC-based resonators*. Journal of Optoelectrical Nanostructures (JOPN). 7(2) (2022) 21-36. Available: <https://doi.org/10.30495/JOPN.2022.29545.1246>
- [26] M. Soroosh, A. Mirali, and E. Farshidi. *Ultra-Fast All-Optical Half Subtractor Based on Photonic Crystal Ring Resonators*. Journal of Optoelectrical Nanostructures (JOPN). 5(1) (2020) 83-100. Available: https://jopn.marvdasht.iau.ir/article_4035.html
- [27] F. Haddadan, M. Soroosh, M. J. Maleki. *Presenting a two-valley Monte Carlo model for simulating and analyzing electron behavior in GaAs bulk and investigating the effects of electron transitions (Gunn Effect)*. 1st international and 7th national conference Congress on Electrical Engineering and Intelligent Systems. Najaf Abad. Iran (2024). Available: <https://civilica.com/doc/1963406/>
- [28] S. M. H. Jalali, M. Soroosh, and Gholamreza Akbarizadeh. *Ultra-fast 1-bit comparator using nonlinear photonic crystal-based ring resonators*. Journal of Optoelectrical Nanostructures (JOPN). 4(3) (2019) 59-72. Available: https://jopn.marvdasht.iau.ir/article_3620.html
- [29] F. Haddadan, M. Soroosh, R. Rajasekar. *Analysis and Simulation of The Schottky Junction Using an Ensemble Monte Carlo Model*. Journal of Optoelectrical Nanostructures (JOPN). 9(3) (2024) 1-17. Available: <https://doi.org/10.30495/jopn.2024.33465.1318>
- [30] F. Haddadan, F. Bagheri, A. Basem, H. A. Kenjrawy, M. Soroosh. *Evanescent field engineering to reduce cross-talk in pattern-free suspended graphene-based plasmonic waveguides using nano-strips*. Optik 313 (2024) 171989. Available: <https://doi.org/10.1016/j.ijleo.2024.171989>
- [31] M. J. Maleki, M. Soroosh, F. Haddadan. *Graphene-Based Optical Waveguides for Surface Plasmon Polariton Transmission*. Optical Waveguide Technology and Applications. IntechOpen. (2024). Available: <https://doi.org/10.5772/intechopen.114810>

- [32] D.M. Sullivan. *Electromagnetic Simulation Using the FDTD Method*. John Wiley & Sons. (2013).
- [33] M.A.K. Othman, C. Guclu, and F. Capolino. *Graphene-based tunable hyperbolic metamaterials and enhanced near-field absorption*. *Opt. Express*. 21(6) (2013) 7614–7632. Available: <https://doi.org/10.1364/OE.21.007614>
- [34] J.R. Piper, and S.H. Fan. *Total absorption in a graphene monolayer in the optical regime by critical coupling with a photonic crystal guided resonance*. *ACS Photonics* 1(4) (2014) 347–353. Available: <https://doi.org/10.1021/ph400090p>
- [35] A. Yadav, M. Danesh, L. Zhong, G.J. Cheng, L. Jiang, and L. Chi. *Spectral plasmonic effect in the nano-cavity of dye-doped nanosphere-based photonic crystals*. *J. Nanotechnol.* 27(16) (2016). Available: <https://doi.org/0.1088/0957-4484/27/16/165703>
- [36] F. Bagheri, M. Soroosh, F. Haddadan, and Y. Seifi-Kavian. *Design and simulation of a compact graphene-based plasmonic D flip-flop*. *Opt. Laser Technol.* 155 (2022) 108436. Available: <https://doi.org/10.1016/j.optlastec.2022.108436>
- [37] F. Haddadan, and M. Soroosh. *Design and simulation of a subwavelength 4-to-2 graphene-based plasmonic priority encoder*. *Opt. Laser Technol.* 157 (2023) 108680. Available: <https://doi.org/10.1016/j.optlastec.2022.108680>
- [38] N.K. Emani, T.F. Chung, A.V. Kildishev, V.M. Shalaev, Y.P. Chen, and A. Boltasseva. *Electrical modulation of Fano resonance in plasmonic nanostructures using graphene*. *Nano Lett.* 14(1) (2014) 78–82. Available: <https://doi.org/10.1021/nl403253c>
- [39] A.R.M. Zain, N.P. Johnson, M. Sorel, and M. Rue. *Ultra high-quality factor one dimensional photonic crystal/photonic wire micro-cavities in silicon-on-insulator (SOI)*. *Opt. Express* 16(16) (2008) 12084–12089. Available: <https://doi.org/10.1364/OE.16.012084>
- [40] H. Yan, X. Li, B. Chandra, G. Tulevski, Y. Wu, M. Freitag, W. Zhu, P. Avouris and F. Xia. *Tunable infrared plasmonic devices using graphene/insulator stacks*. *Nat. Nanotechnol.* 7(5) (2012) 330–334. Available: <https://doi.org/10.1038/nnano.2012.59>
- [41] F. Haddadan, M. Soroosh, A. Basem, H. A. Kenjrawy. *Nano-strip*

Engineering for Coupling Length Enhancement in Pattern-Free Suspended Graphene-based Plasmonic Waveguides. Plasmonics 313 (2024) 171989.
Available: <https://doi.org/10.1007/s11468-024-02541-9>